Journal of Materials Chemistry A

ROYAL SOCIETY OF CHEMISTRY

PAPER

View Article Online
View Journal | View Issue

Cite this: J. Mater. Chem. A, 2025, 13, 22745

N-Heterocyclic carbene-promoted copper powder conditioning for thermal spray applications†

Jashanpreet Kaur, ‡[af] Golnoush Asadiankouhidehkordi, ‡[bf] Vikram Singh, [af] Andre C. Liberati, [bf] Ahmad Diraki, [cf] Souhaila Bendahmane, [cf] Mark D. Aloisio, [df] Payank Patel, [bf] Jeffrey Henderson,[e] Fadhel Ben Ettouil,[b] Cathleen M. Crudden, *[df] Mark Biesinger, *[ef] Annie Levasseur,*[cf] Christian Moreau*[bf] and Janine Mauzeroll *[af]

Received 25th October 2024
Accepted 12th May 2025

DOI: 10.1039/d4ta07631a

rsc.li/materials-a

Copper powder is essential in the thermal spray industry for its excellent thermal and electrical conductivity. However, uncontrolled surface oxide on Cu powder degrades coating performance by weakening inter-particle bonding. This study introduces a novel method using N-heterocyclic carbene (NHC) chemistry to remove surface oxides from Cu powder *via* a one-pot immersion process. NHC functionalization not only eliminates surface oxides but also acts as a capping agent, enhancing the corrosion resistance of the sprayed coatings. Detailed investigations using scanning electron microscopy, X-ray photoelectron spectroscopy, and laser desorption/ionization spectroscopy confirmed the successful NHC treatment. The process was scaled up from gram to kilogram scale, demonstrating its industrial feasibility. Mechanical and corrosion tests show that NHC-treated Cu powder thermal sprayed coatings have superior inter-particle bonding compared to those from untreated-Cu powder. This approach shows great promise for improving the quality of metal powder coatings by effectively removing surface oxides.

Introduction

Thermal spraying comprises a family of industrial coating processes applied to a broad range of components[1] to enhance their surface properties in aerospace, automotive, oil and gas, biomedical, manufacturing, *etc.*[2–4] The use of the high-velocity air-fuel (HVAF) process or other spray processes to deposit Cu particles[2,5–8] has yet to reach its full industrial potential because oxide forms on the surface under ambient conditions in an uncontrolled manner, which is known to increase with storage time[9] and under different spray conditions.[10]

Generally, in the thermal spraying processes, powder particles injected into the flame are heated to a semi-molten state and accelerated to high velocities before they impinge on the substrate.[2,7,11] Upon impact, they undergo plastic deformation, flattening, and bonding to the substrate, and dense coatings are produced with remarkable adherence and minimal thermal degradation.[2,8] In general, metals or alloys form bonds when the fresh metal surface of one particle comes in contact with that of another.[12] In particular, in the HVAF process in which solid particles are sprayed at high speed, the oxide layer on powder particles diminishes the plastic deformation upon impact. This is problematic because different powder oxide thicknesses influence the quality of bonding in the final coating.[5,13,14]

Oxide presence reduces the adhesion with the substrate and cohesion amongst the sprayed particles, which decreases the deposition efficiency of Cu powder and can lead to the deterioration of the thermal and electrical conductivity of the final coating.[15,16] Thus, the development of new surface chemistry to remove copper surface oxide is key to improving the performance of Cu-sprayed coatings. This negative influence of an oxide layer on the surface of the spray particles is present in spraying several other types of metals and alloys.

The removal of copper oxides from planar or particulate surfaces has been studied through H_2 gas treatment,[17] D* and CH_3* radicals,[18] vacuum annealing of coated films[19] or powders,[16,20] glacial acetic acid treatment[21] and acid pickling.[22] While these methods can remove oxide, they lack the ability to

[a]Department of Chemistry, McGill University, Montréal, Québec, H3A 0C7, Canada. E-mail: janine.mauzeroll@mcgill.ca

[b]Department of Mechanical, Industrial and Aerospace Engineering, Concordia University Montreal, Quebec, H3G IM8, Canada. E-mail: christian.moreau@concordia.ca

[c]Département de génie de la construction, École de technologie supérieure, Montréal, Québec, H3C 1K3, Canada. E-mail: annie.levasseur@etsmtl.ca

[d]Department of Chemistry, Queen's University, Kingston, Ontario, K7L 3N6, Canada. E-mail: cruddenc@chem.queensu.ca

[e]Surface Science Western, Western University, 999 Collip Circle, Suite LL31, London, Ontario, N6G 0J3, Canada. E-mail: biesingr@uwo.ca

[f]Carbon to Metal Coating Institute, Queen's University, Kingston, Ontario, K7L 3N6, Canada

† Electronic supplementary information (ESI) available. See DOI: https://doi.org/10.1039/d4ta07631a

‡ These authors contributed equally.

cap the surface and prevent further oxidation. Additionally, any methods requiring ultra-high vacuum conditions are untenable for thermal spray applications.

Organic ligands called N-heterocyclic carbenes (NHCs) have recently been reported to reduce and subsequently functionalize planar copper oxide surfaces.[23–26] NHCs have been shown to interact strongly with a plethora of other metal surfaces including gold,[24,26–28] magnesium,[29] platinum,[30] silver,[26] ruthenium, and cobalt.[31] The resulting NHC-based self-assembled monolayers (SAMs) have been proven to be stable in a range of extreme conditions.[23,27] While thiol-based SAMs have also been studied for their capability to remove surface oxide followed by the formation of a self-assembled monolayer (SAM) on Cu surfaces,[32–34] thiol-based analogs of SAMs are not stable under ambient conditions, especially on reactive surfaces such as Cu,[35,36] thus limiting their applications for ambient and aqueous conditions.

Herein, the ability of a common NHC precursor, 1,3-diisopropyl benzimidazolium hydrogen carbonate (NHC·H_2CO_3) to remove surface oxide from copper powder, stabilize the resulting reduced Cu powder, and be employed on scales appropriate for HVAF experiments is described. The mechanical and corrosion properties of the resulting Cu-sprayed coatings were characterized and demonstrated the potential of carbene chemistry in producing corrosion-resistant Cu-sprayed coatings. Finally, the life cycle assessment (LCA) approach as standardized by ISO (2006)[37,38] was employed to evaluate a one-pot immersion method for creating stable NHC films on Cu powder. As part of a responsible research and innovation process, the goal of the LCA study is to assess the environmental implications of this methodology in the research and development phase, to identify potential environmental hotspots, and to develop a more sustainable process.

Results and discussion

NHC functionalization on the Cu powder surface

The powder was immersed in a 10 mM NHC·H_2CO_3 solution (Scheme 1) in MeOH with stirring for 24 h. Once Cu powder settled at the bottom of the flask, the supernatant solution was removed followed by triturating the powder 3–4 times with MeOH. The NHC·H_2CO_3 functionalizes the Cu powder surface in two steps. In the first step, free carbene is generated from NHC·H_2CO_3 in MeOH, releasing water and carbon dioxide (Scheme 1).[23,39] The generated free carbene reacts with oxidized Cu surfaces to remove Cu surface oxide. In the second step, the freshly exposed Cu metal reacts with the excess NHC in the solution to form a thin protective layer on the Cu surface preventing its re-oxidation. Electrospray ionization-mass spectrometry (ESI-MS) (Fig. S26†) was conducted on the aliquot solution to provide insight into the mechanism of this process. This technique confirms the presence of oxidized NHC fragments at masses 219 (cyclic urea) and 221 (aldehyde) (the structure of fragments is presented in Fig. S26†). It confirms that the free carbene successfully interacts with the oxidized Cu surface, reducing the Cu surface (also proved later by XPS) and simultaneously producing oxidized carbene species. The

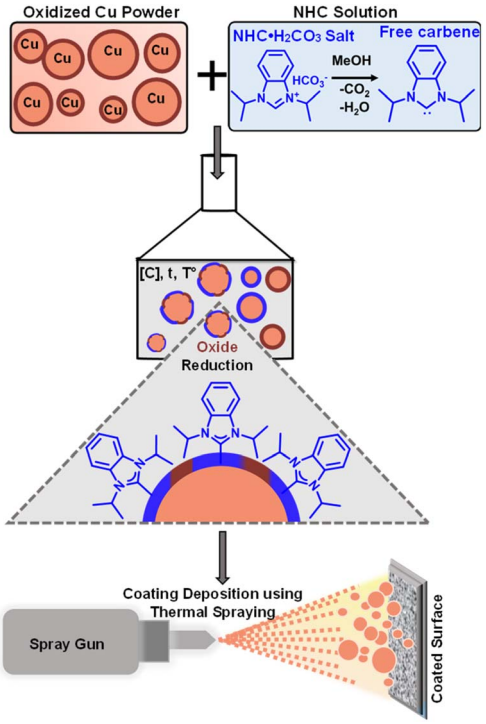

Scheme 1 Schematic representation of the interaction of N-heterocyclic carbene (NHC) with the Cu powder surface resulting in oxide reduction and concurrent formation of a stable NHC film on Cu powder for thermal spray applications.

proposed mechanism is consistent with previous literature studies by Veinot *et al.*[23] and Selva *et al.*[39] on-copper surfaces. After treatment, the Cu particles maintain their spheroidal structure (SEM Fig. 1A and B). The particle size distribution (PSD) assessed *via* dynamic light scattering (DLS) shows no significant disintegration or agglomeration with Dv (50) values of 12.1 μm and 15.2 μm for untreated-Cu and NHC-treated Cu powder, respectively (Table S3 and Fig. S2†). The immersion treatment preserves powder morphology under tested conditions, which is crucial for thermal spray applications.[13,14,40–42]

The presence of an NHC film on the Cu powder was assessed by X-ray photoelectron spectroscopy (XPS) and laser desorption/ionization-time of flight spectroscopy (LDI-ToF). XPS survey spectra were acquired for untreated-Cu and NHC-treated Cu powders (Fig. S5†), showing the presence of expected elements (O, C, N, and Cu). The survey scan analysis confirms the powder purity, with no contaminants observed other than trace amounts of Na and Pb. The atomic ratios of O : C : N were 38 : 36 : 2 for NHC-treated Cu powder *vs.* 41 : 34 : 0.1 for untreated-Cu powder showing a minor change in the O : C ratio and an increase in the N content suggesting the presence of NHC on the Cu powder surface after treatment. High-resolution N 1s spectra (Fig. 1C) show a small signal at a binding energy of 400 eV in the untreated-Cu sample that may be attributed to environmental N_2 interference or sub-surface nitrogen.[23] However, this signal is more significant in NHC-treated Cu samples. To provide more detailed information regarding the source of N on the surface, the LDI-ToF analysis was employed

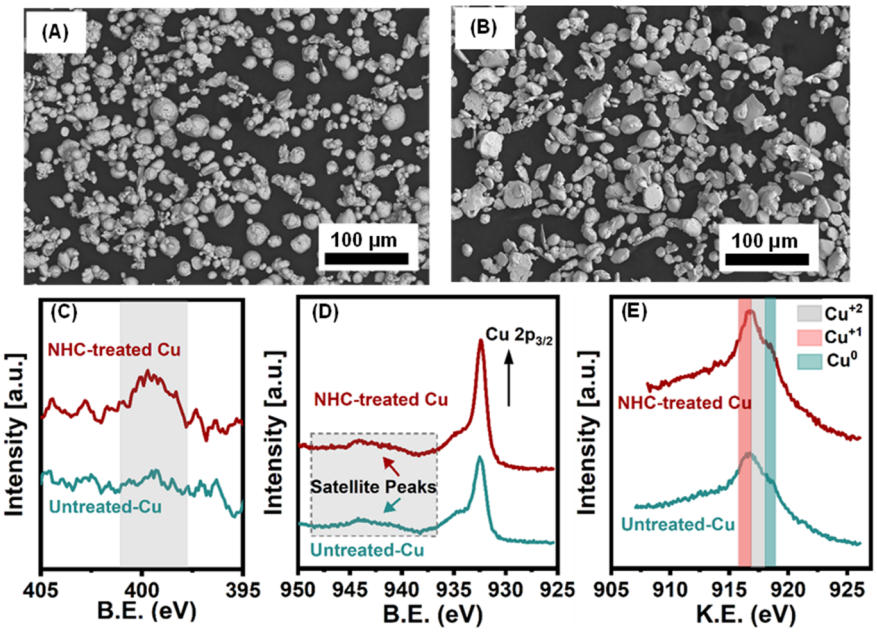

Fig. 1 Microscopic images and spectroscopic measurements performed before and after NHC treatment on Cu powder: (A) and (B) SEM images of untreated-Cu powder *vs.* NHC-treated Cu powder showing no significant disintegration; (C)–(E) N 1s, Cu 2p3/2 and Cu LMM and XPS spectra of untreated-Cu (teal) and NHC-treated Cu (red) powder systems showing the origin of the nitrogen signal after treatment, confirming the NHC presence and the reduction in Cu(II) species.

which enables the observation of intact NHC molecules on the surface. This technique showed the presence of NHC species on the surfaces as $[NHC]^+$ at the expected m/z ratio of 203.[43] No such peak was observed in the untreated-Cu powder (Fig. S6†).

These comparative measurements demonstrate the successful functionalization of NHC on the Cu powder surface under immersion conditions.

Quantitative insight into the surface oxide removal was next obtained using XPS, which provided high-resolution Cu 2p and Cu LMM Auger spectra. The Cu 2p spectra have a main emission line at 932.5 eV attributed to Cu $2p_{3/2}$ which has contributions from Cu(0), Cu(I), and Cu(II), present in untreated-Cu and NHC-treated Cu samples. The shake-up satellite peaks[44] between binding energies of 938 eV and 946 eV are attributed only to Cu(II) species (oxides and hydroxides) and therefore confirm the presence of Cu(II) in untreated-Cu powder samples (Fig. 1D, spectra in teal color). The NHC-treated Cu powder has a suppressed shake-up satellite peak due to Cu(II) reduction (Fig. 1D, spectra in red) consistent with the previously reported work by the Crudden group on Cu polycrystalline surfaces.[23] From the fitting of the Cu 2p signals, the amount of Cu(II) present using the area under the satellite peaks and a combined Cu(0) + Cu(I) can be calculated (details in the Experimental 1.6c section, ESI†).[45,46] The amounts of Cu(II) species calculated to be present on untreated-Cu and NHC-treated Cu were 43% and 31% respectively (Fig. S7A–C, ESI†) reflecting successful oxide reduction by NHC treatment.

The binding energies for Cu(I) and Cu(0) overlap in Cu 2p spectra making it important to analyze the Cu LMM spectra from the Auger region since peaks for Cu(0), Cu(I), and Cu(II) are present at different kinetic energies (K.E.) in these spectra.[45,47] An intense peak for Cu(0) at 918.8 eV K.E. and a reduction in the intensity of the Cu(II) peak at 917.7 eV K.E. were observed for the NHC-treated Cu powder, which is consistent with an increase in metallic species and a decrease in Cu(II) species (Fig. 1E). The Cu LMM Auger peak fittings showed a decrease in Cu(II) species by 10% consistent with Cu 2p fittings and an increase in metallic Cu from 7% to 21% after NHC treatment, based on the average of two independent sets of measurements (Fig. S7D–F, ESI†). Thus, surface oxide reduction occurs reliably and reproducibly after the NHC treatment. It should be noted that these reactions and analyses were conducted under ambient conditions, so some re-oxidation in the environment is expected.

Before scale-up, NHC film deposition conditions were optimized in terms of (1) stirring, (2) NHC concentration, (3) immobilization time, and (4) temperature (Section 1.3 and 2.2 ESI, Fig. S8 to S19†). The Cu LMM Auger spectra fitting was used as a measure of the amount of Cu in different oxidation states (Fig. 2). Optimal conditions were found to be 10 mM NHC concentration and 24 h immersion at room temperature under stirring, which leads to a maximum reduction of Cu(II) species without altering the particle's morphology.

Using these optimized conditions, the chemical stability of NHC-treated *vs.* untreated-Cu powders was assessed before scale-up and thermal spray. Chemical stability tests were conducted in 0.1 M HCl and 0.1 M NaOH solutions. The NHC-treated Cu powder was immersed in each solution for 5 h, and the LDI-ToF mass spectra (Fig. S20†) showed the presence of NHC at 203 m/z even after immersion, indicating a strong Cu-NHC bond and a stable film. Additionally, the Cu powder samples were heated at 100 °C for 36 h in an oxygen-rich environment to test their oxidative stabilities. Under these

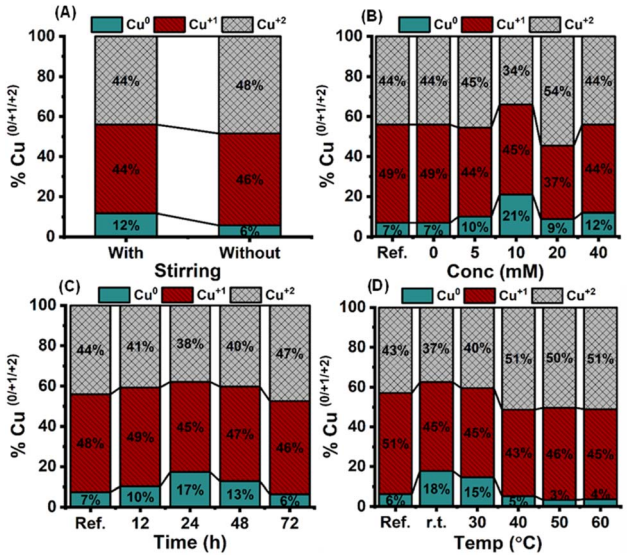

Fig. 2 Optimization of the NHC film on the Cu surface and influence on % of Cu species (0/I/II). The Cu LMM Auger fitting results are presented in a bar graph for (A) stirring, (B) NHC concentration, (C) time of immobilization, and (D) effect of temperature, where ref. stands for the reference sample and r.t. stands for room temperature.

conditions, the untreated-Cu powder turned brown, while the NHC-treated Cu powder showed no significant change in color, suggesting considerable oxidation resistance at high temperatures under an oxygen-rich environment.[14] Post heat-treatment, bulk oxygen measurements were carried out using the ONH elemental analysis (Fig. 3B, grey color) by the inert gas fusion technique, showing a similar amount of bulk oxygen in untreated-Cu powder *vs.* NHC-treated Cu powder, with larger errors for the untreated system. Information regarding surface localized copper oxides was obtained using XPS, revealing a significantly higher shake-up peak area in the Cu 2p spectra of untreated-Cu compared to NHC-treated Cu powder. This confirms the higher oxidation resistance of NHC-treated samples (Fig. 3C and D).

Characterization of thermally sprayed Cu coatings

To produce thermal spray coatings using the untreated-Cu and NHC-treated Cu powder, a thermal spray process using an i7 inner diameter (ID) HVAF gun (Fig. S1, ESI†), with propylene as fuel was employed, with operational parameters summarized in Table S2.† A schematic representation of the thermal spraying process, detailing key components of the HVAF gun and coating events can be found in Fig. 4B (further details are provided in ESI,† in the Experimental section 1.4a–c). Thermogravimetric analysis (TGA) was conducted (Fig. S25†) to understand the evolution of NHC during thermal spraying and its influence on coating composition post-spraying (Table S5†).

The extensive coating build-up process required at least 1.5 kg powder, requiring the scale-up of the synthetic protocol for the production of the NHC precursor (Fig. 4A, precaution; see the Experimental section in ESI†). Quality control for this scaled-up procedure was confirmed by the presence of the NHC peak at 203 *m*/*z* in the LDI mass spectrum (Fig. S21A†) and the reduction in surface oxide using XPS, demonstrating that the optimized immersion conditions are also effective at the kilogram scale (Fig. S21B–F†). The Cu powder was loaded in the spray gun for thermal spraying on carbon steel surfaces to achieve the Cu-sprayed coatings using untreated-Cu and NHC-treated Cu powder. Deposition efficiencies were 60% and 56% respectively[22,48] (calculated using eqn (S1)†), showing similar spraying efficacy. Post-spraying, the bulk and surface oxygen content of the coatings was evaluated using ONH elemental analysis and XPS (Fig. S24†) and O% atomic is presented in Table S4.†

The microstructural, mechanical, and corrosion properties of the resulting coatings were investigated using SEM, electron backscatter diffraction studies (EBSD), scratch tests, and electrochemical impedance (EIS) measurements. SEM cross-section analysis of thermally sprayed coatings reveals uniform, dense coatings with an average thickness of 1.64 mm (untreated-Cu powder – Fig. 4C) and 1.60 mm (NHC-treated Cu powder – Fig. 4D). Coatings generated from the NHC-treated powder (Fig. 4G and H) showed smoother microstructural features compared with untreated-Cu powder (Fig. 4D and E), which indicates better particle deformation under identical spraying conditions, therefore an improved coating.

The crystallographic orientation of the thermal sprayed coatings prepared from NHC-treated Cu powder is characterized using EBSD. It shows more nano-structural well-defined grain boundaries (Fig. 5B) in contrast to coatings from untreated-Cu (Fig. 5A) and the EBSD phase maps are presented in Fig. 5A and B insets showing two distinct phases, Cu in red and oxide in black (detailed explanation in section 2.5 ESI†). This reflects a denser packing and improved adhesion to the carbon steel substrate for NHC-treated copper powder. The cross-section of NHC-treated Cu powder before spraying shows well-defined boundaries (Fig. S22†) indicating that nano-structural features were formed during immersion treatment, not during the thermal spraying process. The NHC plays a crucial role in removing the surface oxide present on the Cu powder and preventing oxidation of the reduced powders, resulting in strong inter-particle bonding and improved coatings.[9,13,14]

The adhesion and cohesion characteristics of untreated-Cu (Fig. 5C) and NHC-treated Cu (Fig. 5D) powder coatings were examined using scratch tests on the sample cross-sections.[49–52] The test may identify two types of failure: adhesive failure at the interface between the substrate and the coating, and cohesive failure within the coating itself. Coatings were subjected to loads ranging from 1 to 6 N, revealing no adhesive failure. Cohesive failure was assessed *via* the cone-shaped fracture created by the indenter, which relates the cone area with the cohesive failure (detailed explanation: Section 1.6f ESI†). The projected cone area (Acn) was calculated using optical microscope images. No significant difference was observed in Acn for both coatings, suggesting similar cohesive strength in both cases (Fig. 5E). The untreated-Cu powder sprayed coating displayed brittle areas along the scratch track, whereas the NHC-treated Cu powder sprayed coating showed material removal,

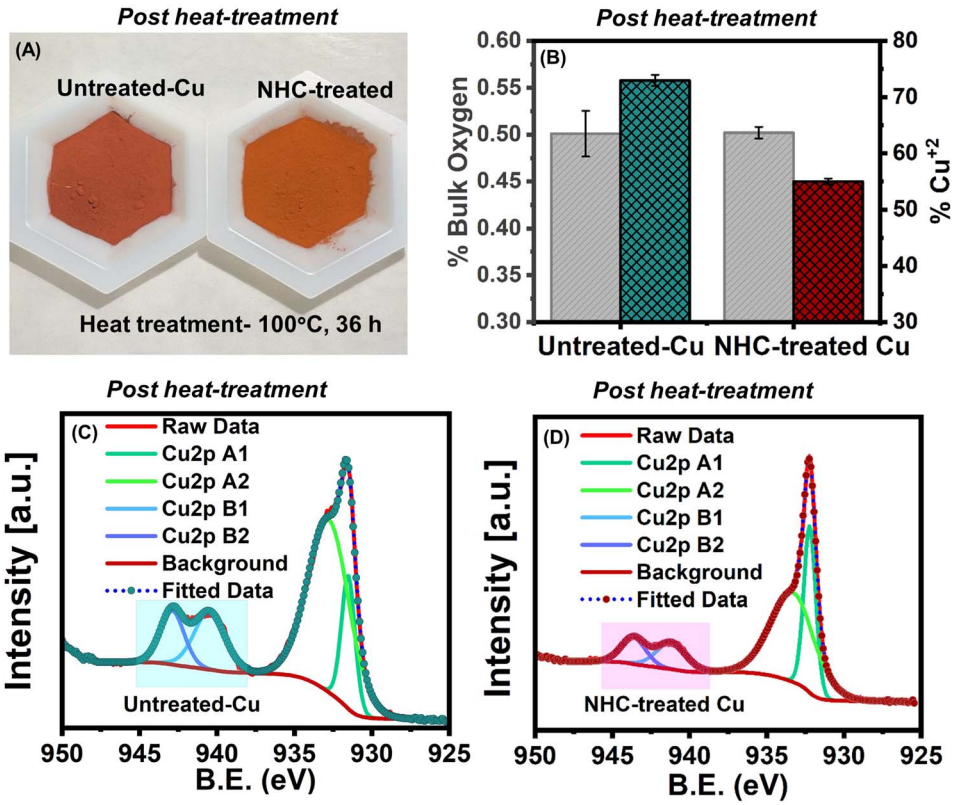

Fig. 3 Thermal stability tests to evaluate the oxidation resistance of untreated-Cu *vs.* NHC-treated Cu powder. (A) Observation in color changes post heat treatment. (B) Bar graph presenting % bulk oxygen using ONH elemental analysis using the inert fusion technique (grey) and surface oxygen measurements using XPS (teal for untreated-Cu and red for NHC-treated Cu powder). (C) and (D) Cu 2p XPS spectra deconvolution for untreated-Cu (teal) *vs.* NHC-treated Cu powder (red).

suggesting a softer microstructure. No cracks or delamination were observed in either coating, indicating overall robustness.

The characteristics of inter-particle bonding and resulting corrosion resistance were evaluated by performing corrosion tests consisting of electrochemical testing followed by microscopic measurements on untreated-Cu and NHC-treated Cu powder sprayed coatings. Before corrosion testing, all coupons were polished using different grades (800, 1200, and 4000) of SiC paper to remove the thick layer of oxide formed during or after the thermal spray process (Fig. S23†). As shown in Fig. 5F, the bigger semicircle in the Nyquist plot for the NHC-treated indicates higher corrosion resistance of the sample towards corrosive media *vs.* untreated-Cu powder sprayed coating. The electrochemical circuit shown in Fig. 5F (inset) was used to fit the obtained data, which is composed of three resistances, R1 (solution resistance), R2 (oxide present on Cu surface), and R3 (the actual charge transfer resistance offered by the Cu-metal).

As can be seen, a higher charge transfer resistance (R_{CT}) of 13 955 Ω (avg of 15 measurements) was observed for the NHC-treated Cu compared to the untreated-Cu (1870 Ω) sprayed surface (Fig. 5G). The higher charge transfer resistance could be explained based on better inter-particle bonding due to the reduced oxide layer for the NHC-treated Cu thermally sprayed surface. This interpretation is supported by focused ion beam scanning electron microscopy (FIB-SEM) experiments to selectively etch the corroded surface (post-corrosion) for both untreated-Cu (Fig. 5H) and NHC-treated Cu powder (Fig. 5I) sprayed coatings. In this experiment, lower penetration of ions was observed for the sprayed coatings from NHC-treated Cu powder. This is also supported by the studies reported by Li *et al.*[22]

Life cycle assessment of the NHC treatment process on Cu powder

Next, the life cycle assessment (LCA) was carried out to evaluate the potential environmental impacts of the immersion method to functionalize Cu powder with NHC and its deposition on steel *via* the thermal spray application process (HVAF) and identify improvement opportunities. LCA provides a systematic methodology for quantifying environmental burdens associated with products, processes, and systems throughout their life cycle, encompassing stages from raw material acquisition to end-of-life management.[53]

The preliminary LCA of the environmental footprint associated with NHC-treated Cu powder immersion treatment and the HVAF application process in Fig. 6 is carried out within the context of Quebec (Canada) (Section 1.5 ESI† for more details). The process's contribution to climate change is expressed in Fig. 6A as equivalent kilograms of carbon dioxide (CO_2) and it releases an equivalent of 18.5 kg CO_2-eq. This unit facilitates

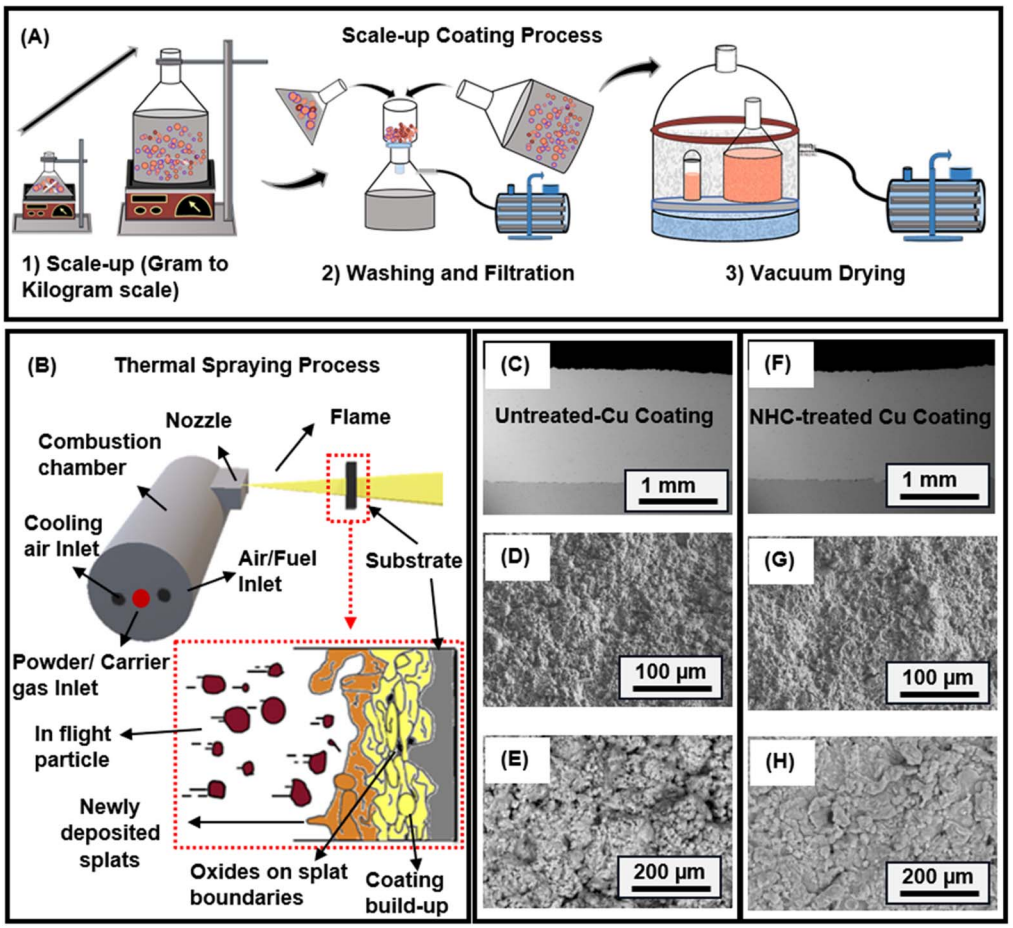

Fig. 4 (A) and (B) Schematic representation of scaling-up for NHC-treated Cu powder and depiction of the thermal spraying process. Microstructure analysis (top view and cross-section view) using SEM for coating build-up using thermal spraying from (C)–(E) untreated-Cu and (F)–(H) NHC-treated Cu powder.

a comparison of the warming effect of various greenhouse gases to CO_2, a common reference point.[54] This analysis shows that the main contributor to the carbon footprint is the production and combustion of propylene for thermal spray. The potential health risks (carcinogenic and non-carcinogenic toxic effects) associated with emitted substances are shown in Fig. 6B and are compared to a reference chemical, 1,4-dichlorobenzene (1,4-DCB).[55] The immersion method has a potential impact equivalent to 80 kg of 1,4-DCB-eq. While the specific NHC used does not appear to be inherently toxic, Cu within the input materials value chains contributes to overall toxic pollutant emissions.[56] The third assessment was done to understand the impact of the process on the depletion of non-renewable mineral resources. This assessment converts the mass of all used minerals to an equivalent amount of Cu as a reference element due to its widespread industrial use,[57] and Fig. 6C (0.23 Cu-eq) indicates the reliance on finite resources in this process.

This holistic approach helps identify improvement opportunities across the product value chain. For instance, adding NHC to Cu powder increases environmental impacts as shown in Fig. 6, but if it leads to a higher lifetime for the coated material, net environmental benefits could occur. The use phase will be added to this LCA model when data on the performance of the coating will be made available. This will allow for a more complete evaluation of the coating's net environmental benefits, considering the potential trade-off between increased short-term impacts and extended product lifetime.

It is also crucial to note that while the quantity of Cu used significantly exceeds that of carbene, their respective environmental impacts on global warming are comparable. This comparison presents a methodological challenge due to the disparate data sources: industrial-scale data for copper (from the Ecoinvent database) *versus* a simplified model for carbene synthesis based on laboratory-scale data for the amounts of energy and materials used. It is anticipated that the development of an industrial-scale carbene production process will lead to optimization in reactant usage, energy consumption, and byproduct valorization. Consequently, the LCA results obtained are expected to be substantially lower for carbene than the current estimates. An additional factor that can significantly improve environmental performance is using a lower amount of NHC-treated Cu powder for coating build-up using an HVAF gun.

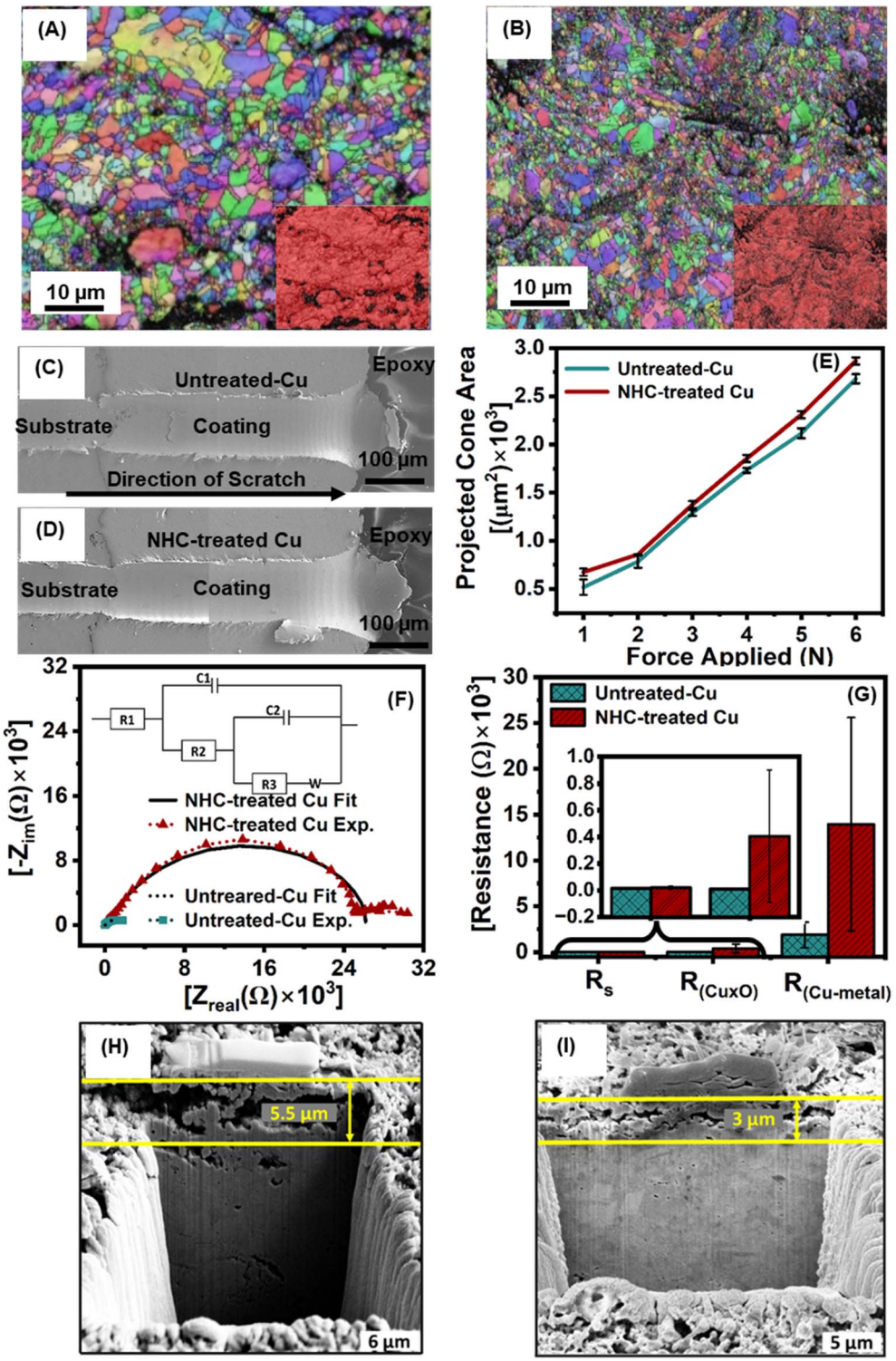

Fig. 5 Mechanical and electrochemical characterization of thermally sprayed coatings generated from untreated-Cu and NHC-treated Cu powder surfaces. EBSD measurements show different nanostructural grain boundaries of thermally sprayed coatings: (A) untreated-Cu and (B) NHC-treated Cu powder over carbon steel surfaces. The EBSD phase maps are presented in (A) and (B) insets showing two distinct phases, Cu in red and oxide in black. (C) and (D) SEM images were acquired after a scratch test at a 6 N load of thermally sprayed coatings from untreated-Cu and NHC-treated Cu powder respectively. (E) Correlation between the applied load during the scratch tests and the projected cone area collected from SEM images for both kinds of surfaces. (F) Nyquist plot resulting from electrochemical impedance spectroscopic (EIS) investigations on both (A) & (B) surfaces represented by teal and red trace respectively, when measured in a corroding aqueous 3.5% NaCl solution at their respective open circuit potential. The inset in (F) shows the EC-circuit used to fit the EIS data. (G) Average resistance values obtained from multiple measurements as depicted in (F). Post-corrosion FIB-SEM acquisitions are shown in (H) & (I) for (A) and (B) sample surfaces respectively, showing ion penetration (thickness of the corroded area) depth being greater for untreated-Cu powder *vs.* NHC-treated Cu powder sprayed thermally *i.e.*, more corrosion resistance is offered by the latter surface.

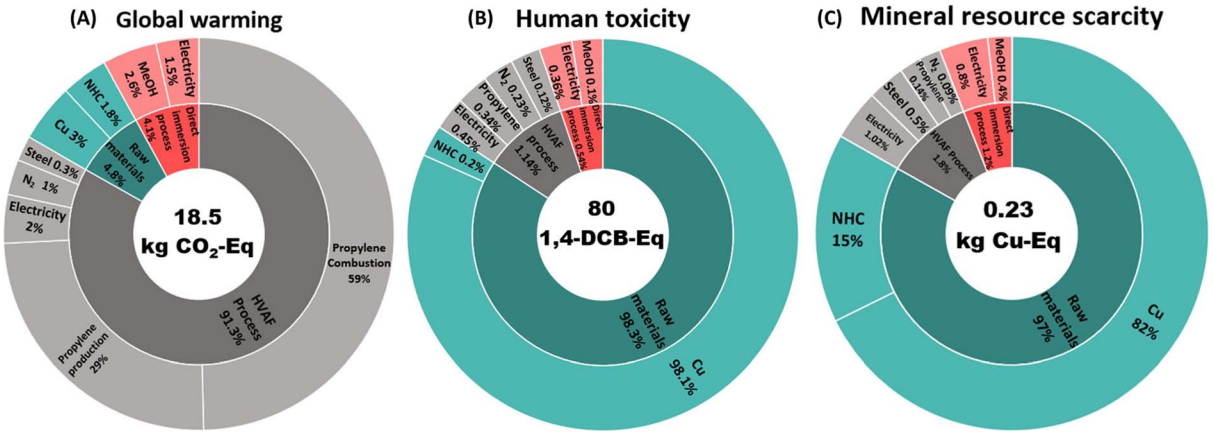

Fig. 6 Environmental impact breakdown analysis of the HVAF thermal spraying of 6 samples (32.7 cm^2 each) of steel using a total of 470 g of Cu powder treated with NHC using the immersion method. The pie chart details the primary environmental impact categories, offering a comprehensive overview of the process' implications: (A) global warming impact ($kgCO_2$-eq), (B) human toxicity potential (kg 1,4-DCB-eq), and (C) mineral resource scarcity potential (kg Cu-eq).

This would reduce the amounts of copper and NHC used, as well as the spray time, which drives the amount of propylene consumed and burned. Although the study focuses on Cu, methanol, and electricity, exploring alternative materials or processes with lower Cu dependence could be valuable for future research.

Conclusions

A reliable, simple, and reproducible one-pot immersion methodology for the reduction of surface oxide and the concurrent formation of an NHC film on Cu powder was successfully developed. The successful surface anchoring of an NHC film on the Cu powder surface was confirmed using XPS and LDI-ToF mass spectroscopy. The maximum increment in metallic features and maximum reduction in surface oxide were observed when 10 mM, 24 h, r.t., and stirring were employed among the examined parameters. Analysis of NHC-treated Cu powder using LDI-ToF mass spectroscopy showed the stability of NHC films under extreme pH conditions. XPS analysis confirmed the oxidation resistance of NHC-treated Cu powder *vs.* untreated-Cu powder at high temperatures under an oxygen-rich environment. The optimized protocol is scalable from gram scale to kilogram scale, with similar film efficiency and reproducibility. HVAF thermal spraying experiments using untreated-Cu and NHC-treated Cu powder produce Cu coatings with thicknesses of approximately 1.6 mm and similar deposition efficiencies. Mechanical strength and corrosion tests were performed after thermal spraying using EBSD, scratch testing, and EIS measurements. Results indicate that thermally sprayed coatings from NHC-treated Cu powder maintain their mechanical properties and show superior corrosion resistance relative to coatings from untreated-Cu powder. The comprehensive LCA study shows potential environmental impacts and helps to develop more sustainable processes. This study establishes a basis to test the NHC-treated powder using other thermal spray techniques such as cold-spray and compare the properties of generated Cu-sprayed coatings with the HVAF system. The future aim is to test different NHC structures that can further improve inter-particle bonding by reducing more oxide and potentially increasing the lifespan of Cu-sprayed coatings.

Data availability

The data are available on request to the corresponding authors.

Author contributions

Jashanpreet Kaur – immersion process, scale-up process, stability tests, XPS including XPS fittings, SEM, DLS measurements, and corresponding evaluation, and wrote, edited, and created figures for the manuscript. Golnoush Asadiankouhidehkordi – thermal spraying, stability test, SEM, DLS, scratch test, EBSD analysis, and wrote, edited, and created figures for the manuscript. Vikram Singh – assisted in the scale-up process. EIS and FIB-SEM measurements, and wrote and edited the manuscript. Andre C. Liberati – assisted in the thermal spray process, and edited the manuscript. Ahmad Diraki – LCA calculations and analysis, and wrote, edited, and created figures for the manuscript. Souhaila Bendahmane – LCA calculations and analysis, and wrote, edited, and created figures for the manuscript. Mark D. Aloisio – synthesized NHC·HCO_3, and edited the manuscript. Payank Patel – scratch test on Cu-sprayed coatings, and edited the manuscript. Jeffrey Henderson – assisted in XPS fittings, and edited the manuscript. Fadhel Ben Ettouil – assisted in the thermal spraying process. Cathleen M. Crudden – conceptualization, editing, reviewing the manuscript and data analysis/interpretation. Mark Biesinger – reviewed XPS fittings and calculations, and edited the manuscript. Annie Levasseur – reviewed LCA calculations and edited the manuscript. Christian Moreau – reviewed thermal spray results, conceptualization, supervision, and data analysis/interpretation. Janine Mauzeroll – conceptualization,

supervision, editing, reviewing the manuscript, and data analysis/interpretation.

Conflicts of interest

The authors declare no conflicts of interest.

Acknowledgements

The authors acknowledge financial support from the NFRF-T Canada (NFRFT-2020-00573). We thank Dr Nadim Saahe for the kind assistance with LDI-ToF-MS measurements (McGill University). We extend our sincere thanks to the Collaborative Research and Training Experience (CREATE) Excellence in Canadian Corrosion Education through Internationalization, Equity, and Interdisciplinarity (CORRECT) program funded by the Natural Sciences and Engineering Research Council of Canada (NSERC) (CREATE 565232-2022) for providing support to this work. NSERC is also thanked for support through discovery grants to the PIs. The Canada Foundation for Innovation and the Canada Research Chairs programs are thanked for their support. J. Kaur and G. Asadiankouhidehkordi have contributed equally to the paper.

References

1 J. R. Davis, *Handbook of Thermal Spray Technology*, ASM international, 2004.
2 M. I. Boulos, P. L. Fauchais and J. V. Heberlein, *Thermal Spray Fundamentals: from Powder to Part*, Springer, 2021.
3 P. L. Fauchais, J. V. Heberlein, M. I. Boulos, P. L. Fauchais, J. V. Heberlein and M. I. Boulos, *Thermal Spray Fundamentals: from Powder to Part*, 2014, pp. 1401–1566.
4 T. N. Rhys-Jones, *Surf. Coat. Technol.*, 1990, **43**, 402–415.
5 G. Asadiankouhidehkordi, A. C. Liberati, F. B. Ettouil and C. Moreau, Inner Diameter High-Velocity Air Fuel (ID-HVAF) Spraying of Copper, Compared to Cold Spray, in *International Thermal Spray Conference*, 2023, pp. 531–537.
6 O. Lanz and B. Gries, HVAF: Chance and Challenge for Users and for Powder Producers, in *Proceedings of the International Thermal Spray Conference*, 2019, pp. 15–22.
7 C. Lyphout and S. Björklund, *J. Therm. Spray Technol.*, 2015, **24**, 235–243.
8 S. Wen, C. Dai, W. Mao, Z. Ren, X. Wang, Y. Zhao and G. Han, *Coatings*, 2022, **12**, 458.
9 M. Razavipour, S. Rahmati, A. Zúñiga, D. Criado and B. Jodoin, *J. Therm. Spray Technol.*, 2021, **30**, 304–323.
10 T. Stoltenhoff, C. Borchers, F. Gärtner and H. Kreye, *Surf. Coat. Technol.*, 2006, **200**, 4947–4960.
11 C. L. Nicolaie Markocsan, L. G. Östergren and M. Sieger, Comparison between High-Velocity-Air-Fuel-(HVAF) and Cold-Gas-Spray (CGS) by evaluating mechanical properties of Ti-6-4-and INCONEL718-coatings, *Report INCO718*, 2011, pp. 2–16.
12 N. F. Kazakov, *Diffusion Bonding of Materials*, Elsevier, 2013.
13 C.-J. Li, H.-T. Wang, Q. Zhang, G.-J. Yang, W.-Y. Li and H. Liao, *J. Therm. Spray Technol.*, 2010, **19**, 95–101.
14 X.-T. Luo, Y. Ge, Y. Xie, Y. Wei, R. Huang, N. Ma, C. S. Ramachandran and C.-J. Li, *J. Mater. Sci. Technol.*, 2021, **67**, 105–115.
15 W.-Y. Li, C.-J. Li and H. Liao, *Appl. Surf. Sci.*, 2010, **256**, 4953–4958.
16 K. Ko, J. Choi and H. Lee, *J. Mater. Process. Technol.*, 2014, **214**, 1530–1535.
17 J. Y. Kim, J. A. Rodriguez, J. C. Hanson, A. I. Frenkel and P. L. Lee, *J. Am. Chem. Soc.*, 2003, **125**, 10684–10692.
18 P. Kirsch and J. Ekerdt, *J. Appl. Phys.*, 2001, **90**, 4256–4264.
19 S. Lee, N. Mettlach, N. Nguyen, Y. Sun and J. White, *Appl. Surf. Sci.*, 2003, **206**, 102–109.
20 K. Ko, J. Choi, H. Lee and B. Lee, *Powder Technol.*, 2012, **218**, 119–123.
21 K. Chavez and D. Hess, *J. Electrochem. Soc.*, 2001, **148**, G640.
22 Y.-J. Li, X.-T. Luo and C.-J. Li, *Surf. Coat. Technol.*, 2021, **407**, 126709.
23 A. J. Veinot, A. Al-Rashed, J. D. Padmos, I. Singh, D. S. Lee, M. R. Narouz, P. A. Lummis, C. J. Baddeley, C. M. Crudden and J. H. Horton, *Chem.–Eur. J.*, 2020, **26**, 11431–11434.
24 C. R. Larrea, C. J. Baddeley, M. R. Narouz, N. J. Mosey, J. H. Horton and C. M. Crudden, *ChemPhysChem*, 2017, **18**, 3536–3539.
25 I. Berg, E. Amit, L. Hale, F. D. Toste and E. Gross, *Angew. Chem., Int. Ed.*, 2022, **134**(25), e202201093.
26 L. Jiang, B. Zhang, A. Paavo Seitsonen, F. Haag, F. Allegretti, J. Reichert, B. Kuster, J. V. Barth and A. C. Papageorgiou, *Chem. Sci.*, 2017, **8**(12), 8301–8308.
27 C. M. Crudden, J. H. Horton, I. I. Ebralidze, O. V. Zenkina, A. B. McLean, B. Drevniok, Z. She, H. B. Kraatz, N. J. Mosey, T. Seki, E. C. Keske, J. D. Leake, A. Rousina-Webb and G. Wu, *Nat. Chem.*, 2014, **6**, 409–414.
28 A. Krzykawska, M. Wróbel, K. Kozieł and P. Cyganik, *ACS Nano*, 2020, **14**, 6043–6057.
29 L. Stephens, J. D. Padmos, M. R. Narouz, A. Al-Rashed, C.-H. Li, N. Payne, M. Zamora, C. M. Crudden, J. Mauzeroll and J. H. Horton, *J. Electrochem. Soc.*, 2018, **165**, G139.
30 Y. Zeng, T. Zhang, M. R. Narouz, C. M. Crudden and P. H. McBreen, *Chem. Commun.*, 2018, **54**, 12527–12530.
31 J. T. Lomax, E. Goodwin, M. D. Aloisio, A. J. Veinot, I. Singh, W.-T. Shiu, M. Bakiro, J. Bentley, J. F. DeJesus and P. G. Gordon, *Chem. Mater.*, 2024, **36**(11), 5500–5507.
32 C. A. Calderon, C. Ojeda, V. A. Macagno, P. Paredes-Olivera and E. M. Patrito, *J. Phys. Chem. C*, 2010, **114**, 3945–3957.
33 D. A. Hutt and C. Liu, *Appl. Surf. Sci.*, 2005, **252**, 400–411.
34 M. M. Sung, K. Sung, C. G. Kim, S. S. Lee and Y. Kim, *J. Phys. Chem. B*, 2000, **104**, 2273–2277.
35 Y. Wang, J. Im, J. W. Soares, D. M. Steeves and J. E. Whitten, *Langmuir*, 2016, **32**, 3848–3857.
36 J. B. Schlenoff, M. Li and H. Ly, *J. Am. Chem. Soc.*, 1995, **117**, 12528–12536.
37 I. ISO14040, *Environmental Management—Life Cycle Assessment—Principles and Framework*, 2006, pp. 235–248.
38 I. Standard, *Environmental Management-Life Cycle Assessment-Requirements and Guidelines*, ISO, 2006.
39 J. S. G. Selva, Y. Li, J. Kaur, A. Juneau, A. Diraki, S. Bendahmane, J. D. Henderson, M. D. Aloisio, A. Messina

and A. Nezamzadeh, *ACS Appl. Mater. Interfaces*, 2025, 10004–10014.
40 Y.-J. Li, X.-T. Luo and C.-J. Li, *Surf. Coat. Technol.*, 2017, **328**, 304–312.
41 J.-T. Liang, S.-F. Chang, C.-H. Wu, S.-H. Chen, C.-W. Tsai, K.-C. Cheng and K. Hsu, *Coatings*, 2023, **13**, 1065.
42 W. Wong, P. Vo, E. Irissou, A. Ryabinin, J.-G. Legoux and S. Yue, *J. Therm. Spray Technol.*, 2013, **22**, 1140–1153.
43 A. J. Veinot, A. Al-Rashed, J. D. Padmos, I. Singh, D. S. Lee, M. R. Narouz, P. A. Lummis, C. J. Baddeley, C. M. Crudden and J. H. Horton, *Chem.–Eur. J.*, 2020, **26**(50), 11431–11434.
44 J. F. Watts and J. Wolstenholme, *An Introduction to Surface Analysis by XPS and AES*, John Wiley & Sons, 2019.
45 M. C. Biesinger, *Surf. Interface Anal.*, 2017, **49**, 1325–1334.
46 M. C. Biesinger, B. R. Hart, R. Polack, B. A. Kobe and R. S. C. Smart, *Miner. Eng.*, 2007, **20**, 152–162.
47 J. Chastain and R. C. King Jr, *Handbook of X-ray photoelectron spectroscopy*, Perkin-Elmer Corporation, 1992, vol. 40(221), p. 25.
48 Y. Li, Y. Wei, X. Luo, C. Li and N. Ma, *J. Mater. Sci. Technol.*, 2020, **40**, 185–195.
49 J. Nohava, B. Bonferroni, G. Bolelli and L. Lusvarghi, *Surf. Coat. Technol.*, 2010, **205**, 1127–1131.
50 P. Patel, V. N. V. Munagala, N. Sharifi, A. Roy, S. A. Alidokht, M. Harfouche, M. Makowiec, P. Stoyanov, R. R. Chromik and C. Moreau, *J. Mater. Sci.*, 2024, **59**, 4293–4323.
51 C. Sha, Z. Zhou, Z. Xie and P. Munroe, *Surf. Coat. Technol.*, 2019, **367**, 30–40.
52 C. Sha, Microstructure, mechanical properties, scratch responses and wear behaviours of transition metal nitride and high entropy alloy coatings, *Chuhan Sha School of Materials Science and Engineering*, 2020.
53 M. A. Curran, *Overview of Goal and Scope Definition in Life Cycle Assessment*, Springer, 2017.
54 K. Armour, P. Forster, T. Storelvmo, W. Collins, J. L. Dufresne, D. Frame, D. Lunt, T. Mauritsen, M. Palmer, M. Watanabe and M Wild, The earth's energy budget, climate feedbacks, and climate sensitivity, in *Climate Change*, 2021, pp. 923–1054.
55 T. E. McKone and E. G. Hertwich, *Int. J. Life Cycle Assess.*, 2001, **6**, 106–109.
56 M. Pohanka, *Bratisl. Lek. Listy*, 2019, **120**, 397–409.
57 A. Beylot, J. Dewulf, T. Greffe, S. Muller and G.-A. Blengini, *Int. J. Life Cycle Assess.*, 2024, **29**, 890–908.